Supporting Information

Real-World Emission of Particles from Vehicles: Volatility and the Effects of Ambient Temperature

Jonathan M. Wang,[†] Cheol-Heon Jeong,[†] Naomi Zimmerman,[†] Robert M. Healy,[‡] Nathan Hilker,[†] Greg J. Evans[†]*

[†]Department of Chemical Engineering and Applied Chemistry, University of Toronto, Toronto, Ontario M5S3E5 Canada

[‡]Environmental Monitoring and Reporting Branch, Ontario Ministry of the Environment and Climate Change, Etobicoke, Ontario M3P3V6 Canada

Corresponding author:
Jonathan M. Wang
Dept. of Chemical Engineering and Applied Chemistry
University of Toronto
200 College Street, Room 123, Toronto, Canada, M5S 3E5
Tel. 416-978-5932
Fax. 416-978-8605
Email. jonm.wang@utoronto.ca

14 pages, 5 tables, 4 figures

S1: Sampling and Instrument Details

The site and measurement setups are similar to a previous study Wang et al. (2015) and will be summarized below for clarity.[1] Inlets were located 15 m from the roadway and 3 m above the ground where ambient air was continuously drawn. Gaseous pollutants were drawn through 2 m of 0.953 cm Teflon fluorinated ethylene propylene (FEP) tubing and split through a glass manifold to the gas analyzers. Measurements were made using two identical chemiluminescence analyzers, one set to NO mode and the other to NO_x mode; a gas filter correlation infrared analyzer for CO, and a non-dispersive infrared analyzer for CO_2 (42i, 48i, and 410i, respectively; Thermo Scientific, Waltham, MA) (Table S1). The time resolution for NO, NO_x, and CO_2 measurements was 1 s, and for CO measurements was 10 s.

A separate dedicated inlet was used for VOC sampling using a 0.635 m Teflon FEP line. A proton transfer reaction time-of-flight mass spectrometer (PTR-TOF-MS, model 8000, IOINCON, Analytik, Innsbruck, Austria) was connected to the line upstream of a pump providing a make-up flow of 3 lpm. The PTR-TOF-MS was operated similar to Jordan et al. with H3O+ as the reagent ion, a mass range up to m/z 452, and a 2 s time resolution.[2] Individual VOCs were calibrated for using two standard mixtures made by the National Air Pollution Surveillance Network at Environment Canada based on the United States Environmental Protection Agency (U.S. EPA) TO15 method for 150 non-polar VOCs and 40 independently chosen polar OVOCs. Data was processed using PTR-MS Viewer 3.1.0.20 and converted from counts per second to mass concentration using the corresponding 6-level calibration curve.

For the particle-phase pollutant measurements, a 10 cm stainless steel tube inlet with a 2.5 µm cut-off was used with an input flow of 170 l min^{-1}. Measurements were made using a photoacoustic soot spectrometer for particle absorption at 781 nm (PASS-3, Droplet Measurement Techniques, Boulder, CO); a condensation particle counter (CPC, model 651, Teledyne Advanced Pollution Instrumentation, San Diego, CA) for total particle number (PN) concentration, which has a particle range of 7 - 2500 nm; a fast mobility particle sizer (FMPS, model 3091, TSI Inc., Shoreview, MN) for size-resolved particle number concentration with particles between 5.6 – 856 nm; and a photoelectric aerosol sensor (PAS 2000, EcoChem, League City, TX) for particle-bound polycyclic aromatic hydrocarbons (Table S1). Measurement time resolutions were 1 s for the FMPS, 2 s for the PASS-3 and CPCs, and 6 s for the PAS2000.

In addition to measurements made at high time resolution for calculating emission factors, supplementary measurements at lower time resolution were used to convert the optical signals from the PASS-3 to mass concentrations for various components of ambient aerosol. Particle absorption coefficient (B_{abs}, λ = 781 nm) measurements were converted to mass concentration by linear correlation with coincident 2 hour integrated measurements made with a thermal-optical organic carbon-elemental carbon analyzer (Sunset Lab OC-EC, Sunset Laboratories, Inc., Tigard, OR).[3] The calculated mass absorption cross sections, used to convert the absorption (Mm^{-1}) to mass concentration (µg m^{-3}) was 3.2, 3.7, 3.8, 3.7 m^2 g^{-1} for fall, winter, spring, and summer campaigns, respectively, and is specific to the study conditions and instrumentation.

Table S1: Summary of measurement site instrumentation and the corresponding sensitivity, range, precision and time resolution.

Parameter	Instrument Type	Model	Effective Sensitivity[a]	Range (Precision)[b]	Time Res.
CO_2	Non-dispersive infrared gas analyzer	410i	5 ppmv	0 – 1000 ppmv (±1%)	1 s
CO	Filter correlation infrared gas analyzer	48C	150 ppbv	0 – 10 ppmv (±0.1 ppmv)	10 s
NO, NO_x	Chemiluminescence analyzer	42i	3 ppbv	0 – 500 ppbv (±0.4 ppbv)	1 s
Particle Number	Condensation Particle Counter	651 [c]	1500 # cm^{-3}	0 – 10^6 # cm^{-3} (±10%)	2 s
Particle Number and Size Distribution	Fast Mobility Particle Sizer	3091[d]	2000 # cm^{-3}	0 – 10^7 # cm^{-3} (±3%)	1 s
Particle Absorption (781 nm)	Photoacoustic Soot Spectrometer	PASS-3	8 Mm^{-1}	0 – 100,000 Mm^{-1} (±3.0 Mm^{-1})	2 s
Particle Absorption (405 nm)			50 Mm^{-1}	0 – 100,000 Mm^{-1} (± 10 Mm^{-1})	
Particle Scattering (405 nm)			15 Mm^{-1}	0 – 100,000 Mm^{-1} (± 10 Mm^{-1})	
VOCs	PTR-TOF-MS	8000	0.2 - 1 ppbv[e]	10 pptv – 1 ppmv (±0.1 ppbv)[a]	2 s
Particle-bound PAHs	Photoelectric Aerosol Sensor	2000	14 ng m^{-3}	0 – 1000 ng m^{-3} (±5%)[a]	6 s
Thermodenuder System[f]					
Particle Number	Condensation Particle Counter[g]	3788	400 # cm^{-3}	0 – 4×10^5 # cm^{-3} (±1%)[g]	2 s
Supplementary Measurements[h]					
Elemental Carbon	Thermal-optical OC/EC	Sunset OC/EC		0 – 15 µg cm^{-3} (±4-6%)	2 h
Organic Aerosol	Aerosol Mass Spectrometer	ACSM[i]		N/A (±0.4 ug/m^3)	30 min
$PM_{2.5}$	Nephelometry/radio metric mass monitor	SHARP 5030		0 – 1000 µg m^{-3} (±2 µg m^{-3})	1 min

[a] Average effective sensitivity calculated from all campaigns, [b] instrumental precision provided by manufacturer specifications except for PTR-TOF-MS and PAS2000 which was unavailable, alternative precision was calculated as 3σ from measurement of zero air, [c] particle size range of 7 – 2500 nm, [d] particle size range of 6.5 – 856 nm, [e] effective sensitivity range for BTEX, [f] effective sensitivity calculated for particle measurements post-thermodenuder, [g] particle size range of 2.5 – 2500 nm, [h] precision is for 10,000 # cm^{-3}, where $\sigma = (\sqrt{N}/N) \times 100\%$ defined by manufacturer, [h] effective sensitivity column simply manufacturer defined sensitivity for supplementary measurements, [i] particle size range ~40 – 1000 nm

S2: Instrument Intercomparison of PASS-3, ACSM, and SP-AMS

Particle scattering coefficient (B_{sca}, λ = 405 nm) measurements were first corrected for influence from black carbon using Eq. 3 defined in the main text. This corrected scattering coefficient was converted to organic aerosol by multiple linear correlation with coincident 30 minute integrated measurements made by an aerosol chemical speciation monitor (ACSM, Aerodyne Research Inc., Billerica, MA), with an instrument size cut-off at ~50 nm. Operations and calibration of the ACSM is described in Jeong et al. (2016).[4] The results from the multiple linear regression between the PASS-3 B_{sca} and ACSM measurements of organic aerosol (OA), sulfate (SO_4), and nitrate (NO_3) is summarized in Table S2. Vehicle exhaust of particles are made predominantly of carbonaceous material, as seen in previous studies and described by Dallmann et al. (2014).[5] Assuming that negligible amounts of sulfate and nitrate exists in the vehicle plume, background subtracted B_{sca} values should be mainly influenced by OA, a mass scattering cross-section (MSC) of 3.4 $m^2\ g^{-1}$ can be used to convert the integrated scattering coefficient within the plume to OA mass concentration (Table S2).

Table S2: Results from multiple linear regression of PASS-3 vs. ACSM OA+SO_4+NO_3, with an adjusted R^2 = 0.988.

Parameter	Slope (±95% CI)	p-value
OA	3.37 ± 0.13	$<2\times10^{-16}$
SO_4	9.58 ± 0.40	$<2\times10^{-16}$
NO_3	5.96 ± 0.33	$<2\times10^{-16}$

S3: Thermodenduer System Loss Range

Particle loses from the thermodenuder system (TD) were calculated by comparing ambient CPC measurements with coinciding CPC measurements downstream of the TD turned off, with average particle losses of 32%. However, it was found when coinciding measurements were made with an FMPS upstream and downstream of a similar TD setup of diluted vehicle exhaust sampled described in more detail in Zimmerman et al., that particle losses in the TD system ranged between an estimated 19 – 56%.[6] Differences as a result of the different loss corrections are provided in Table S3.

Table S3: Range of PN_{TD} EF and percent PN volatiles values based on different TD system loss values.

	TD System Line Loss		
Variable	**32%**	**19%**	**56%**
Mean PN_{TD} EF	0.51×10^{14}	0.47×10^{14}	0.61×10^{14}
Percent PN Volatilized	94%	94%	92%
Mean PN_{TD} EF (PN-emitters only)	0.72×10^{14}	0.65×10^{14}	0.83×10^{14}
Percent PN Volatilized (PN-emitters only)	93%	94%	92%
Separated by Season			
Mean PN_{TD} EF (summer)	0.43×10^{14}	0.40×10^{14}	0.48×10^{14}
Mean PN_{TD} EF (winter)	0.65×10^{14}	0.59×10^{14}	0.77×10^{14}
Percent PN Volatilized (summer)	87%	88%	86%
Percent PN Volatilized (winter)	94%	95%	93%

S4: Conversion for Distance-Based Emission Factors from In-Lab Studies

Most in-lab dynamometer and some on-road vehicle emission studies report in distance-based emission factors (EF_{db}), typically in per mile or per km units, which can roughly be converted into fuel-based emission factors (EF_{fb}) by using the fuel economy provided for the vehicle or assuming an combined average value based on the vehicle type of one is not reported (source: https://www.fueleconomy.gov/ or equivalent source). An average density was assumed for diesel (ρ_{diesel} = 0.832 kg/L) and gasoline (ρ_{gas} = 0.74 kg/L; average between 0.70 – 0.78 kg/L).

With a fuel economy of 27.4 MPG (US), an adjusted combined cycle fuel economy for an average 2015 GDI vehicle, a conversion factor can be calculated by:

$$\mathrm{EF_{fb}(g/kg) = EF_{db}(g/mi)} \times \frac{27.4\ \mathrm{mi}}{\mathrm{gal}} \times \frac{\mathrm{gal}}{3.79\ \mathrm{L}} \times \frac{\mathrm{L}}{0.740\ \mathrm{kg}}$$

$$\mathrm{EF_{fb}(g/kg) = EF_{db}(g/mi)} \times \frac{9.77\ \mathrm{mi}}{\mathrm{kg}}$$

Now, using 0.0858 L/km as the equivalent metric fuel economy unit, the conversion factor is:

$$\mathrm{EF_{fb}(g/kg) = EF_{db}(g/km)} \times \frac{\mathrm{km}}{0.0858\ \mathrm{L}} \times \frac{\mathrm{L}}{0.740\ \mathrm{kg}}$$

$$\mathrm{EF_{fb}(g/kg) = EF_{db}(g/km)} \times \frac{15.8\ \mathrm{km}}{\mathrm{kg}}$$

Table S4: Summary of emission factors that required conversion from distance-based EFs, values taken assume normal operating conditions.

Vehicle	Veh. Type	Mode	Fuel Eco.	EF_{db}	EF_{fb}	EF_{db}	EF_{fb}
Karavalakis et al.[7] (Chassis Dyno.; CVS; Instr. CPC 3772 (>10 nm), CPC 3776 (>2.5 nm), MAAP; Fuel: E10 – E15; in miles)							
				PN (# 10^{14})		**BC**	
Honda Civic (2007)	PFI	UC	28.85	0.02	0.20	0.1	1.2
Dodge Ram (2007)	PFI		12.7	0.04	0.17	0.3	1.4
Toyota Camry (2012)	PFI		26.9	0.05	0.45	0.1	1.0
Toyota Optima (2012)	GDI		26.7	0.08	0.80	0.8	7.3
Chevrolet Impala (2012)	GDI		21.4	0.05	0.41	0.6	4.6
Honda Civic (2007)	PFI	FTP	31.2	0.01	0.14	0.1	1.6
Dodge Ram (2007)	PFI		13.7	0.03	0.13	0.3	1.5
Toyota Camry (2012)	PFI		28.45	0.04	0.40	0.1	0.9
Toyota Optima (2012)	GDI		27.45	0.07	0.70	0.8	7.8
Chevrolet Impala (2012)	GDI		20.9	0.05	0.34	0.6	4.6
Maricq et al.[8] (Chassis Dyno.; CVS; Instr. CPC 3010 (>10 nm); Fuel: E10; in miles)							
Vehicle 1 (2010)	GDI	FTP	24[a]	0.84 – 5.5	0.07 – 0.47		
Vehicle 2 (2010)	GDI		24[a]	2.1 – 6.7	0.18 – 0.57		
Chan et al.[9] (Chassis Dyno.; CVS; Instr. EECPC 3790 (>23 nm), MicroAeth; Fuel: E0 – E10; in miles)							
Hyundai Sonata (2011)	GDI	FTP	26	0.07	0.60	8.0	74.3
Volvo S40 (2010)	PFI		24	0.01	0.06	0.3	2.6
Ford Focus (2012)	GDI		31	0.10	1.11	5.2	57.5
Ford Transit Connect (2013)	PFI		24	0.01	0.09	0.9	7.7
Hyundai Sonata (2011)	GDI	US06	26	0.02	0.19	2.4	22.3
Volvo S40 (2010)	PFI		24	0.00	0.01	0.2	1.7
Ford Focus (2012)	GDI		31	0.10	1.06	4.5	49.8
Ford Transit Connect (2013)	PFI		24	0.22	1.88	0.6	5.1
Karjalainen et al.[10] (Chassis Dyno.; porous tube diluter & short aging chamber; EEPS (>5.6 nm) & UCPC 3025 (>3 nm), ELPI (>6 nm); in km; fuel eco. in mpg)							
Vehicle 1 (2011)	GDI	UDC	24[a]	0.06 – 0.07	0.76 – 0.95		
		EUDC	24[a]	0.07 – 0.16	1.0 – 2.1		
		NEDC	24[a]	0.07 – 0.12	0.9 – 1.7		

[a] averaged from Karavalakis et al. GDI FTP fuel economies

Table S4: Continued.

Vehicle	Veh. Type	Mode	Fuel Eco.	EF_{db}	EF_{fb}		
Karavalakis et al.[11] (Chassis Dyno.; CVS; Instr. GC-MS; Fuel: Diesel; in km)							
				PAH (µg)	**PAH (ng)**		
Toyota Corrola (1998)	Diesel	NEDC	0.053	130	3.31		
		ADC	0.089	102	1.54		
Alves et al.[12] (Chassis Dyno.; CVS; Instr. GC-MS; in km, fuel eco. in mpg)							
Euro 3 (2004)	PFI	ARTEMIS	34.5	89 – 226	0.68 – 1.73		
Euro 4 (2006)	PFI		37	0.1 – 41	0.001 – 0.3		
Euro 5 (2012)	PFI		40	0.4 – 3.9	0.003 – 0.03		
Euro 3 (2003)	Diesel		37.3	392 – 430	2.89 – 3.17		
Euro 4 (2006)	Diesel		37	1.2 – 1.4	0.009 – 0.01		
Euro 4 (2009)	Diesel		41	0 – 12	0 – 0.096		
Perrone et al.[13] (Chassis Dyno.; Dilution tunnel; GC-MS; in km)							
Euro 1	Diesel	IT, UDC, EUDC	0.07	26.8	0.50		
Euro 2	Diesel		0.08	3.1	0.05		
Euro 3	Diesel		0.08	1.3	0.02		
Euro 1	PFI		0.10	5.0	0.07		
Euro 3	PFI		0.07	0.3	0.01		
Euro 1	Diesel		0.09	15.3	0.22		
Euro 2	Diesel		0.07	10.4	0.19		
Euro 2	Diesel		0.10	2.1	0.02		
Euro 3	Diesel		0.07	2.7	0.05		
Euro 4	Diesel		0.10	1.4	0.02		

Abbreviations for Table S4:
PFI: Port Fuel Injection Light-Duty Gasoline Vehicle
GDI: Gasoline-Direct Injection Light-Duty Vehicle
CVS: Constant Volume Sampler
UC: Unified Cycle (CARB)
FTP: Federal Test Procedure (U.S. EPA)
US06: Supplemental Federal Test Procedure (U.S. EPA)
UDC: Urban Driving Cycle (UNECE)
EUDC: Extra-Urban Driving Cycle (UNECE)
NEDC: New European Driving Cycle (UNECE)
ADC: Athens Drive Cycle
ARTEMIS: Artemis Drive Cycle
IT: Non-Conventional Intense Traffic Mode

S5: Sample PN_{nonTD} and PN TD measurements

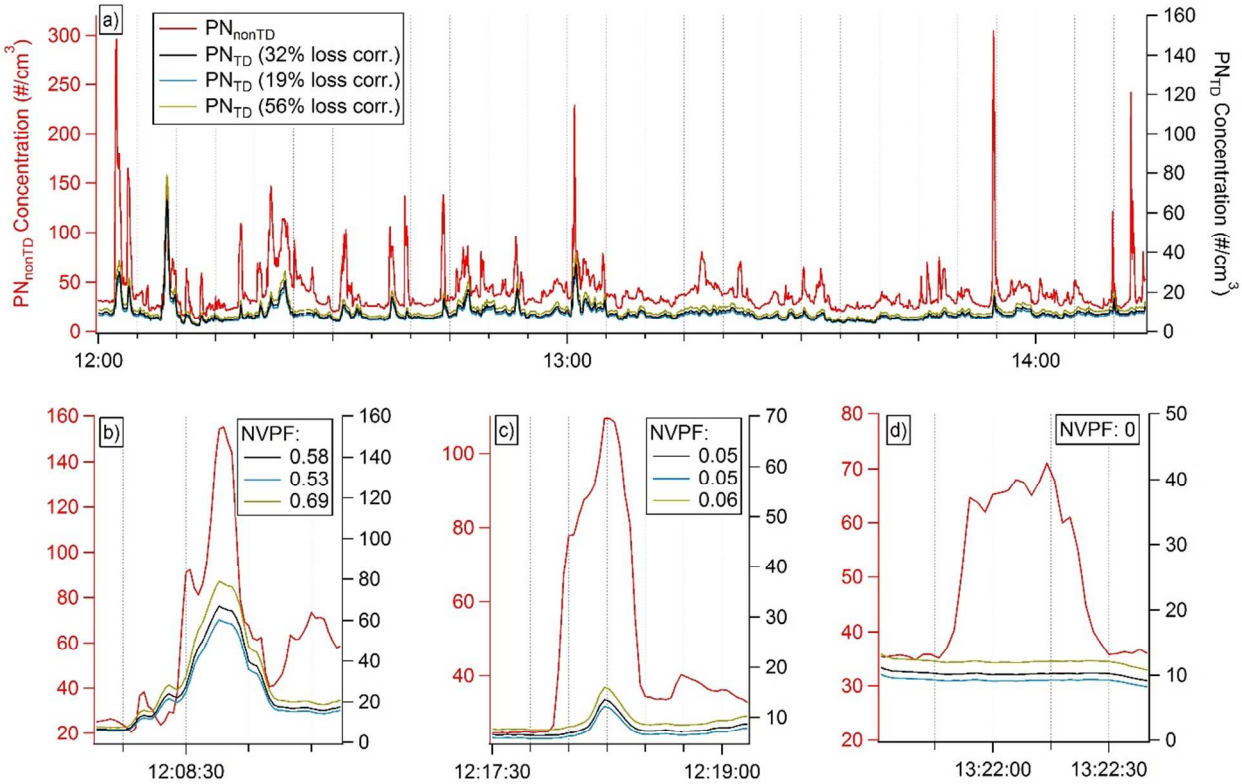

Figure S1: Sample time series of PN_{nonTD} and PN_{TD} concentration (a), with example PN plumes with higher (b), medium (c), and low (d) NVPF fraction. Axis scales are different depending on plume.

S6: Particle Size Distribution Size Categories

Given that the NVPF with the largest particle size included many of the heavy emitting vehicles, mean pollutant EFs associated with the dominant particle size of plumes were also investigated. Plumes were categorized as undetected or as one of two particle size categories based on their background-subtracted mean mode diameters (MMD): MMD <60 nm, or ≥60 nm (Figure S2a). Plumes with a total particle count less than 2000 # cm^{-3} above the background, the effective sensitivity defined for the FMPS (Table S1) in the Supporting Information, were categorized with undetectable particle emissions or "non-PN". Size categories from small to large made up 61% and 3% of the total number of plumes respectively, where 36% were non-PN plumes. Thus plumes with predominantly larger particles represented only 3% of the total. Prior to including only two size categories in this analysis, three and four size categories were explored. However, the resultant mean pollutant EFs of the mid-sized categories had negligible differences and were merged into one (<60 nm).

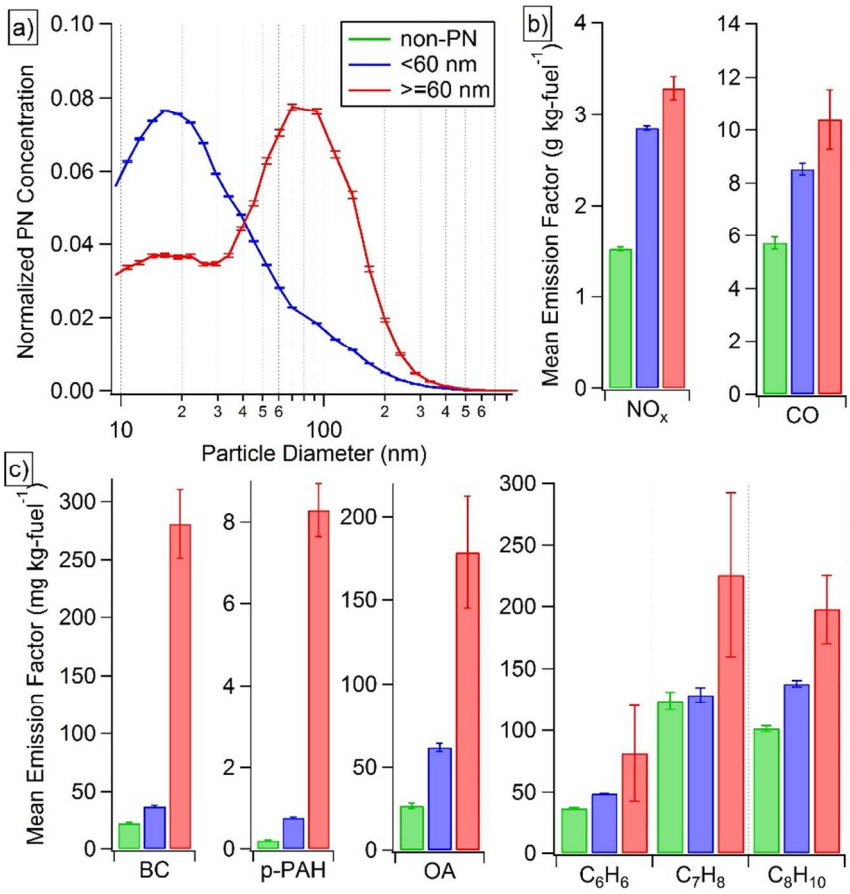

Figure S2: Background-subtracted plume size distributions for <60 nm (blue) and ≥60 nm (red) size categories (a), with corresponding mean EFs for NO_x and CO (b), and BC, p-PAH, OA, and BTEX (c) including a category for plumes with non-detectable PN EFs (green). Error bars indicate 95% confidence interval.

Mean EFs were higher on average for all pollutants in the ≥60 nm category, where BC, p-PAH, and OA EFs were 7.5, 11, and 2.9 times higher than the <60 nm category respectively (Figure S2c). Although typically HDDVs have been found to emit at MMDs >60 nm in dynamometer studies,[14] higher mean CO and BTEX EFs found in this study in the larger size category imply some contribution from LDGVs as well. Not surprisingly, the non-detectable PN category EFs were lower on average for most pollutants except for C_7H_8, which was similar in value to the <60 nm category. C_7H_8 emissions are indicative of gasoline-fueled vehicles, and although some of these vehicles may have undetectable PN emissions, some of these vehicles emit measureable levels of gaseous pollutants.

The above analysis included only two size categories, the original analysis included four categories with size bins of <15 nm, 15 – 30 nm, 30 – 70 nm, and >70 nm, however similar trends were observed as the two category analysis, the number of smaller size categories (<70 nm) were merged as the pollutant EFs had negligible differences (Figure S3). This was especially the case for CO, BTEX, and BC; although mean OA EFs for 30 – 70 nm was significantly different.

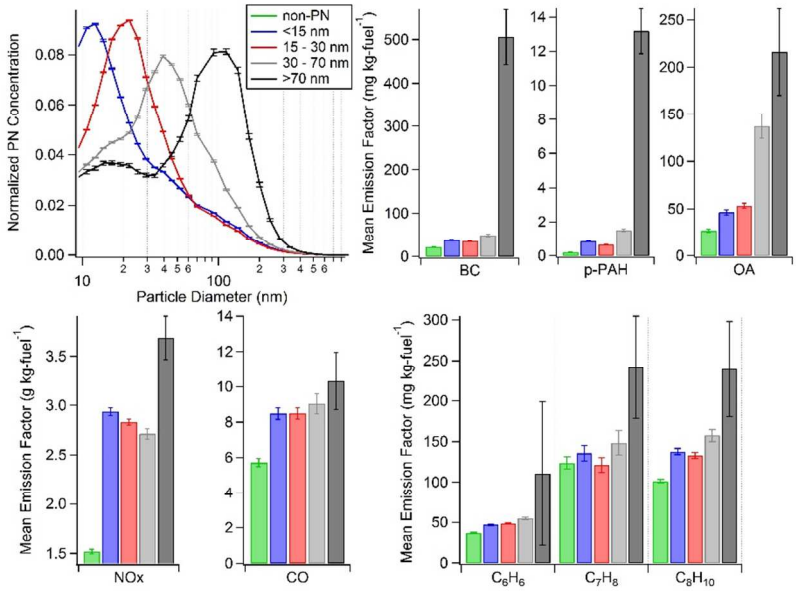

Figure S3: Mean EFs categorized by mean mode diameter from background-subtracted plume size distributions. Error bars indicate 95% confidence interval.

The next step was three size categories, which also resulted in similar EFs in the smaller size categories (Figure S4). The largest size category was shifted to a lower size cutoff to include a larger percentage of plumes, as <1% of the plumes were >70 nm. Shifting of this cutoff did not result in significant changes, and a compromise was met between a reasonable large particle size cutoff and inclusion of a higher percentage of plumes at >60 nm. With negligible difference again in the <15 nm and 15 – 60 nm size categories, these were merged into one.

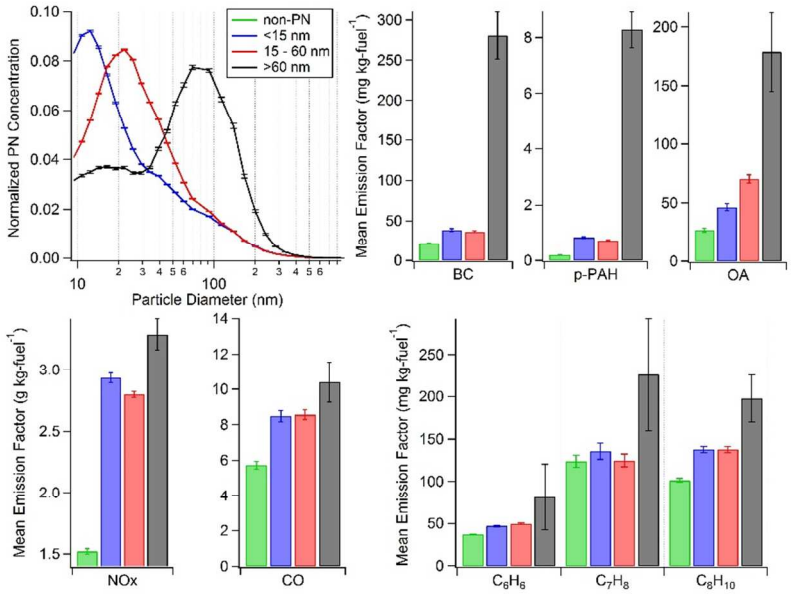

Figure S4: Mean EFs categorized by mean mode diameter from background-subtracted plume size distributions. Error bars indicate 95% confidence interval.

With the evolution of the diesel vehicle fleet and the combinations of different emission control technologies, it has become increasingly difficult to assign HDDVs plumes to one specific emission profile in real-world measurements. For example, the use of a diesel oxidation catalyst (DOC), diesel particulate filter (DPF), and/or selective catalytic reduction (SCR) can result in a variety emission profiles from HDDVs. Modelled and laboratory results of diesel vehicle emissions have found that increased levels of BC emitted at the tailpipe have a considerable suppresive effect on nucleation from condensible organic vapors post-tailpipe.[15] Results from this study support these results; when mean BC EFs increased with increasing NVPF, PN_{nonTD} EFs decreased. Additionally, only a small fraction of particles remained downstream of the thermodenuder for the larger portion of the fleet that emitted higher levels of PN, as similarly found by Saari et al. for HDDVs.[16] A difficult class of vehicles to tease out from this data set is GDI vehicles, which emit significantly higher levels of BC and volatile particles as PN relative to traditional port-fuel injection vehicles,[6, 9] where plumes from GDIs could be categorized in the MVP category.

S7: Percentage HDDV-Influenced Periods

Time periods before the plume start-time were specified as a 90 second time window based on maximum travel time from individual vehicle analysis, where the typical travel time of a plume from tailpipe to the measurement inlet was 20-60 seconds, but based on single vehicle observations extended at times to 90 seconds. The random selection analysis used was two sets of random subsets, with approximately 126 plumes in each analysis (Table S5). The first random subset was chosen, and the subsequent one was selected similarly but excluded any of the first subset data. The percent HDDV-influenced periods for both size categories were similar for the random subsets, however there was a slight decrease in difference for the second random subset.

Table S5: Summary of percentage of HDDV-influenced periods, number of plumes, and ambient temperature separated by random data subsets.

Pollutant	**HDDV-influenced periods (%)**		**Number of Plumes**		**Ambient Temperature (°C)**	
	<60 nm	>60 nm	<60 nm	>60 nm	<60 nm	>60 nm
Random 1	35%	57%	65	61	1.2	12.7
Random 2	36%	54%	64	63	4.4	12.0
Random 3	34%	51%	61	61	0.2	12.5

REFERENCES

1. Wang, J. M.; Jeong, C. H.; Zimmerman, N.; Healy, R. M.; Wang, D. K.; Ke, F.; Evans, G. J., Plume-based analysis of vehicle fleet air pollutant emissions and the contribution from high emitters. *Atmos. Meas. Tech.* **2015,** *8*, (8), 3263-3275.
2. Jordan, A.; Haidacher, S.; Hanel, G.; Hartungen, E.; Märk, L.; Seehauser, H.; Schottkowsky, R.; Sulzer, P.; Märk, T. D., A high resolution and high sensitivity proton-transfer-reaction time-of-flight mass spectrometer (PTR-TOF-MS). *International Journal of Mass Spectrometry* **2009,** *286*, (2–3), 122-128.
3. Knox, A.; Evans, G. J.; Brook, J. R.; Yao, X.; Jeong, C. H.; Godri, K. J.; Sabaliauskas, K.; Slowik, J. G., Mass Absorption Cross-Section of Ambient Black Carbon Aerosol in Relation to Chemical Age. *Aerosol Sci. Technol.* **2009,** *43*, (6), 522-532.
4. Jeong, C. H.; Wang, J. M.; Evans, G. J., Source Apportionment of Urban Particulate Matter using Hourly Resolved Trace Metals, Organics, and Inorganic Aerosol Components. *Atmos. Chem. Phys. Discuss.* **2016,** *2016*, 1-32.
5. Dallmann, T. R.; Onasch, T. B.; Kirchstetter, T. W.; Worton, D. R.; Fortner, E. C.; Herndon, S. C.; Wood, E. C.; Franklin, J. P.; Worsnop, D. R.; Goldstein, A. H.; Harley, R. A., Characterization of particulate matter emissions from on-road gasoline and diesel vehicles using a soot particle aerosol mass spectrometer. *Atmos. Chem. Phys.* **2014,** *14*, (14), 7585-7599.
6. Zimmerman, N.; Wang, J. M.; Jeong, C.-H.; Ramos, M.; Hilker, N.; Healy, R. M.; Sabaliauskas, K.; Wallace, J. S.; Evans, G. J., Field Measurements of Gasoline Direct Injection Emission Factors: Spatial and Seasonal Variability. *Environ. Sci. Technol.* **2016,** *50*, (4), 2035-2043.
7. Karavalakis, G.; Short, D.; Vu, D.; Villela, M.; Asa-Awuku, A.; Durbin, T. D., Evaluating the regulated emissions, air toxics, ultrafine particles, and black carbon from SI-PFI and SI-DI vehicles operating on different ethanol and iso-butanol blends. *Fuel* **2014,** *128*, 410-421.
8. Maricq, M. M.; Szente, J. J.; Adams, J.; Tennison, P.; Rumpsa, T., Influence of Mileage Accumulation on the Particle Mass and Number Emissions of Two Gasoline Direct Injection Vehicles. *Environ. Sci. Technol.* **2013,** *47*, (20), 11890-11896.
9. Chan, T. W.; Meloche, E.; Kubsh, J.; Brezny, R., Black Carbon Emissions in Gasoline Exhaust and a Reduction Alternative with a Gasoline Particulate Filter. *Environ. Sci. Technol.* **2014,** *48*, (10), 6027-6034.
10. Karjalainen, P.; Pirjola, L.; Heikkilä, J.; Lähde, T.; Tzamkiozis, T.; Ntziachristos, L.; Keskinen, J.; Rönkkö, T., Exhaust particles of modern gasoline vehicles: A laboratory and an on-road study. *Atmos. Environ.* **2014,** *97*, (0), 262-270.
11. Karavalakis, G.; Stournas, S.; Bakeas, E., Light vehicle regulated and unregulated emissions from different biodiesels. *Sci. Total Environ.* **2009,** *407*, (10), 3338-3346.
12. Alves, C. A.; Barbosa, C.; Rocha, S.; Calvo, A.; Nunes, T.; Cerqueira, M.; Pio, C.; Karanasiou, A.; Querol, X., Elements and polycyclic aromatic hydrocarbons in exhaust particles emitted by light-duty vehicles. *Environmental Science and Pollution Research* **2015,** *22*, (15), 11526-11542.
13. Perrone, M. G.; Carbone, C.; Faedo, D.; Ferrero, L.; Maggioni, A.; Sangiorgi, G.; Bolzacchini, E., Exhaust emissions of polycyclic aromatic hydrocarbons, n-alkanes and phenols from vehicles coming within different European classes. *Atmos. Environ.* **2014,** *82*, 391-400.

14. Maricq, M. M.; Chase, R. E.; Xu, N.; Laing, P. M., The Effects of the Catalytic Converter and Fuel Sulfur Level on Motor Vehicle Particulate Matter Emissions: Light Duty Diesel Vehicles. *Environ. Sci. Technol.* **2002,** *36*, (2), 283-289.
15. Pirjola, L.; Karl, M.; Rönkkö, T.; Arnold, F., Model studies of volatile diesel exhaust particle formation: are organic vapours involved in nucleation and growth? *Atmos. Chem. Phys.* **2015,** *15*, (18), 10435-10452.
16. Saari, S.; Karjalainen, P.; Ntziachristos, L.; Pirjola, L.; Matilainen, P.; Keskinen, J.; Rönkkö, T., Exhaust particle and NOx emission performance of an SCR heavy duty truck operating in real-world conditions. *Atmos. Environ.* **2016,** *126*, 136-144.